Increased probability of compound long-duration dry and hot events in Europe during summer (1950–2013)

Colin Manning, Martin Widmann, Emanuele Bevacqua, Anne van Loon, Douglas Maraun, Mathieu Vrac

Increased probability of compound long-duration dry and hot events in Europe during summer (1950–2013)

Environmental Research Letters

LETTER

Increased probability of compound long-duration dry and hot events in Europe during summer (1950–2013)

Colin Manning[1,4], **Martin Widmann**[1], **Emanuele Bevacqua**[2], **Anne F Van Loon**[1], **Douglas Maraun**[2] **and Mathieu Vrac**[3]

[1] University of Birmingham, Edgbaston, Birmingham, B152TT, United Kingdom
[2] Wegener Center for Climate and Global Change, University of Graz, Graz, Austria
[3] Laboratoire des Sciences du Climat et de l'Environnement, (LSCE-IPSL), Centre d'Etudes de Saclay, Gif-sur-Yvette, France
[4] Author to whom any correspondence should be addressed.

E-mail: colin.manning@ncl.ac.uk

Keywords: compound event, drought, heat wave, copula

OPEN ACCESS

RECEIVED
24 February 2019

REVISED
17 May 2019

ACCEPTED FOR PUBLICATION
22 May 2019

PUBLISHED
29 August 2019

Abstract

The propagation of drought from meteorological drought to soil moisture drought can be accelerated by high temperatures during dry periods. The occurrence of extremely long-duration dry periods in combination with extremely high temperatures may drive larger soil moisture deficits than either extreme occurring alone, and lead to severe impacts. In this study, we propose a framework to both characterise long-duration meteorological droughts that co-occur with extremely high temperatures and quantify their probability. We term these events as long-duration, dry and hot (*DH*) events and characterise them by their duration (*D*) and magnitude (*M*). *D* is defined as the consecutive number of days with precipitation below 1 mm, while *M* is the maximum daily maximum temperature during an event. A copula-based approach is then employed to estimate the probability of *DH* events. The framework is applied to Europe during the summer months of June, July and August. We also assess the change in probability that has occurred over the historical period 1950–2013 and find an increased probability of *DH* events throughout Europe where rising temperatures are found to be the main driver of this change. Dry periods are becoming hotter, leading to an increase in the occurrence of long-duration dry periods with extremely high temperatures. Some parts of Europe also show an increased probability of long-duration events although the relative change is not as strong as that seen with temperature. The results point to a predominant thermodynamic response of *DH* events to global warming and reaffirm previous research that soil moisture drought events are setting in faster and becoming more severe due to a change in the contributing meteorological hazards. It is hoped that the framework applied here will provide a starting point for further analysis of *DH* events in other locations and for the assessment of climate models.

1. Introduction

Soil moisture drought is a complex hazard (Seneviratne 2012) that can adversely affect crop yields and natural ecosystems. Understanding its relationship with rising global temperatures and changes in precipitation is of significant societal importance. Sparse soil moisture data networks make it a difficult phenomenon to investigate empirically (Robock *et al* 2000, Dorigo *et al* 2011), and forces one to study output from land surface models (Mitchell *et al* 2004, Sheffield *et al* 2014) or observations of the more widely available meteorological drivers, namely precipitation and temperature. In this study, we focus on the meteorological drivers and assess changes in meteorological drought events that co-occur with extreme temperatures, where meteorological drought is defined as an extended dry period. We term such co-occurrences as long-duration, dry and hot (*DH*) events and characterise them by their duration (*D*) and magnitude (*M*). *D* is calculated as the number of consecutive dry days with precipitation below 1mm,

while M is the maximum daily maximum temperature during the given meteorological drought.

The persistence of meteorological drought leads to the propagation of drought into soil moisture resulting in a negative moisture anomaly in the upper layers of soil known as the root zone. This propagation depends on both D and M. Longer dry periods allow for more drying of soil than shorter intermittent dry periods separated by wet days providing recharge, while high temperatures that increase evapotranspiration (ET) can accelerate this propagation of drought (Orlowsky and Seneviratne 2012, Seneviratne *et al* 2012, Teuling *et al* 2013). The joint occurrence of extremely long-duration and high magnitude events may thus lead to higher soil moisture deficits than events where only one characteristic is extreme. Larger deficits can produce longer lasting soil moisture droughts as higher amounts of precipitation are then required for drought recovery (Seneviratne *et al* 2012, Manning *et al* 2018).

The co-occurrence of extremes, such as meteorological drought and high temperatures, is known as a compound event. This 'refers to the combination of multiple meteorological/climatic drivers and/or hazards that contribute to societal or environmental risk' (Zscheischler *et al* 2018). Events involving the co-occurrence of dry and hot extremes are receiving increased attention due to the growing awareness of the severity of their impacts (Ciais *et al* 2005, Shaposhnikov *et al* 2014), which can be far greater than those arising from one extreme alone (Hegerl *et al* 2011, Zscheischler *et al* 2014). Considering such extremes as independent of one another can result in an underestimation in the probability of their co-occurrence (Zscheischler and Seneviratne 2017), as well as in the risk of low crop yields (Zscheischler *et al* 2017), and the probability of wildfires (Gudmundsson *et al* 2014, Ruffault *et al* 2016). Additionally, both the duration and magnitude of dry and hot periods are required to explain the severity of ecosystem impacts (von Buttlar *et al* 2017). Underlying the significance of these studies are findings of increased concurrences of drought and heat waves within the US (Mazdiyasni and AghaKouchak 2015) and India (Sharma and Mujumdar 2017) along with projected increases in the likelihood of dry and hot summers globally (Zscheischler and Seneviratne 2017).

With soil moisture drought events expected to set in quicker and become more severe in a warmer climate (Trenberth *et al* 2014, Samaniego *et al* 2018), it is important to understand the characteristics of *DH* events, D and M, and how they react to a warming climate. With regards to D, an increasing frequency of long-duration events has been seen in the Netherlands (Zolina *et al* 2013), while only small changes were found in the annual maximum duration over Europe (Donat *et al* 2013). Ye (2018) showed increases in the seasonal mean duration across Russia and demonstrated that locations with the largest increases exhibit a higher rise in seasonal mean temperature. However little attention has been given to quantifying the probability of long-duration and high magnitude *DH* events. Many studies have estimated the probability of co-occurring dry and hot conditions (e.g. AghaKouchak *et al* 2014, Zscheischler and Seneviratne 2017, Zscheischler *et al* 2017), though these studies investigate precipitation accumulations over specified periods of time (e.g. monthly, seasonal etc), and not the duration of events which has an important influence on ecosystem impacts (von Buttlar *et al* 2017).

Furthermore, drought analysis based on meteorological variables has for the most part focussed on trends in drought indices such as the SPI (Gudmundsson and Seneviratne 2016), SPEI (Stagge *et al* 2017) and PDSI (Dai *et al* 2004, Sheffield *et al* 2012, Dai 2013, Trenberth *et al* 2014). These indices are calculated by integrating variables such as precipitation and potential ET over time, and so bear no explicit information of individual *DH* events. We therefore look to add further insight to changes in the meteorological hazards that influence soil moisture drought through analysing *DH* events.

In this study, following recommendations of Zscheischler *et al* (2018), we propose a framework to that can be used to characterise compound *DH* events and quantify their probability through the application of a copula-based approach introduced in Bevacqua *et al* (2018). This framework can be applied in other regions and in the assessment of climate model output. We apply the framework to Europe during June, July and August (JJA), and assess the change in probability of *DH* events over the historical period (1950–2013), in terms of their duration, magnitude and co-occurrence of extremes in D and M. By doing so, we aim to gauge the response of such events to climate change and highlight regions that may have a higher risk of impacts due to changes in *DH* events.

2. Data and methods

2.1. Data

For the identification of *DH* events, we use temperature and precipitation data from the EOBS dataset (Haylock *et al* 2008) version 16.0 on a 0.25° grid. EOBS is the state of the art gridded dataset for Europe, although it is produced from a network of stations whose density is heterogeneous in both time and space. Herrera *et al* (2018) point to a minimum number of stations required for reliable grid cell averages when assessing precipitation extremes, which is far higher than that used to produce EOBS in many regions (see Herrera *et al* 2018). However, the events studied here are driven by large-scale systems that will produce smoother fields than localised precipitation extremes, and so we consider EOBS to be adequate for identifying the events of interest.

The dataset is available from 1950 to 2017, although data is missing over Russia from 2014 onwards. We therefore analyse the period of 1950 until and including 2013 to keep a consistent time period throughout Europe. There are also many missing values of precipitation over Poland, Iceland and parts of Northern Africa throughout the observation period. These areas are therefore removed from the analysis. We also employ the ERA Interim reanalysis dataset (Dee *et al* 2011) to provide temperature data for the composite plots presented in figure 1, as EOBS is a land-only dataset.

2.2. Event definition

We characterise *DH* events by their duration (D) and magnitude (M) and identify events occurring within June, July and August (JJA). Events overlapping these months that begin before or end after this period are also included. D is defined as the number of days where precipitation is consecutively below 1 mm. This threshold is chosen to remain consistent with previous studies (Orlowsky and Seneviratne 2012, Donat *et al* 2013, Sillmann *et al* 2013, Lehtonen *et al* 2014), as well as to be applicable to output from climate models which systematically overestimate the number of drizzle days. To ensure we obtain an independent event set (Coles *et al* 2001) and capture events in their entirety (Fleig *et al* 2006), we combine events longer than the 90th percentile of duration that are separated by $n_{sep} = 2$ days or less. Combining events shorter than the 90th percentile can result in events made up of intermittent dry and wet periods rather than the distinct dry events that we seek. The choice of two days is a subjective choice, and the sensitivity of the results to this choice was tested with values of $n_{sep} = 0, 1, 2, 3,$ and 4 days. Little difference is seen between results obtained for each value of n_{sep} and so this choice will not affect the overall message of the paper.

M is defined as the maximum daily maximum temperature observed during a dry period, it is thus defined separately to D. M is highly correlated with the mean of the maximum daily maximum temperatures during an event and so it is taken to represent the level of temperature throughout each event. Although temperature is not the sole driver of the atmospheric evaporative demand for water, it is the main driver of changes in atmospheric evaporative demand through alterations to vapour pressure deficits (Scheff and Frierson 2014, Zhao and Dai 2015), and is more widely available than other variables. We therefore assume that it provides us with an indication of potential changes in the drying of soil moisture during *DH* events over time.

2.3. Estimation of univariate and bivariate return periods (RPs)

The univariate RP for a dry period of a given duration is the average waiting time between dry periods of at least that duration, while the univariate RP for a given magnitude is the average waiting time between events with at least that magnitude. We estimate univariate RPs for an exceedance of a given value of each characteristic (D and M) separately. RPs are quantified using a peak over threshold (PoT) approach in which stationary parametric models are applied to exceedances of the thresholds d_{sel}^{uni} and m_{sel}^{uni} (*sel*: selected, *uni*: univariate) for D and M respectively (see appendices for details on threshold selection). The univariate RP, T, of an event exceeding a duration d is estimated as (Coles *et al* 2001):

$$T(d) = \frac{\mu_D}{1 - F(d)}, \quad (1)$$

where $1 - F(d)$ is the probability of an event exceeding a duration d, F is the cumulative distribution function (CDF) of the exceedances above d_{sel}^{uni}, while μ_D is the mean inter-arrival time between events with a duration exceeding d_{sel}^{uni}. This is estimated as $\mu_D = N_Y/N_E$, where N_Y is the number of years in the observation period and N_E is the total number of exceedances of d_{sel}^{uni}. The RP of an event exceeding a magnitude of m, $T(m)$, is estimated in the same manner.

A bivariate RP provides the estimated expected waiting time between events in which specified values of D and M are jointly exceeded. Following the approach in Bevacqua *et al* (2018), bivariate RPs are estimated through a PoT approach in which a parametric copula-based probability distribution is applied to events in which D and M jointly exceed their respective thresholds d_{sel}^{bi} and m_{sel}^{bi} (*sel*: selected, *bi*: bivariate). This ensures we focus on long-duration dry and hot events.

A copula is a multivariate distribution function that models the dependence between random variables independently of the marginal distributions. According to Sklar (1959), the joint distribution of D and M may be written as:

$$F(D, M) = C(u_D, u_M), \quad (2)$$

where C is the copula modelling the dependence between the selected (D, M) pairs while $u_D = F_D(d)$ and $u_M = F_M(m)$ are uniformly distributed variables on [0, 1]. F_D and F_M are respectively the marginal CDFs of D and M from events with joint exceedances. The bivariate RP of an event exceeding D_q and M_q is then estimated as (Salvadori *et al* 2007):

$$T(D_q, M_q) = \frac{\mu_E}{1 - u_{D_q} - u_{M_q} + C(u_{D_q}, u_{M_q})}, \quad (3)$$

where $\mu_E = N_Y/N_E$ is the average inter-arrival time of events where D and M jointly exceed the thresholds d_{sel}^{bi} and m_{sel}^{bi}, and $u_{D_q} = F_D(D_q)$ (likewise for u_{M_q}).

We estimate univariate and bivariate RPs in two separate time periods, a reference (*ref* : 1950–1979) and a present (*pres*: 1984–2013) period. We quantify the change in RPs from *ref* to *pres* and estimate the contributions to these changes from variations in D, M and the (D, M) dependence. For details on the

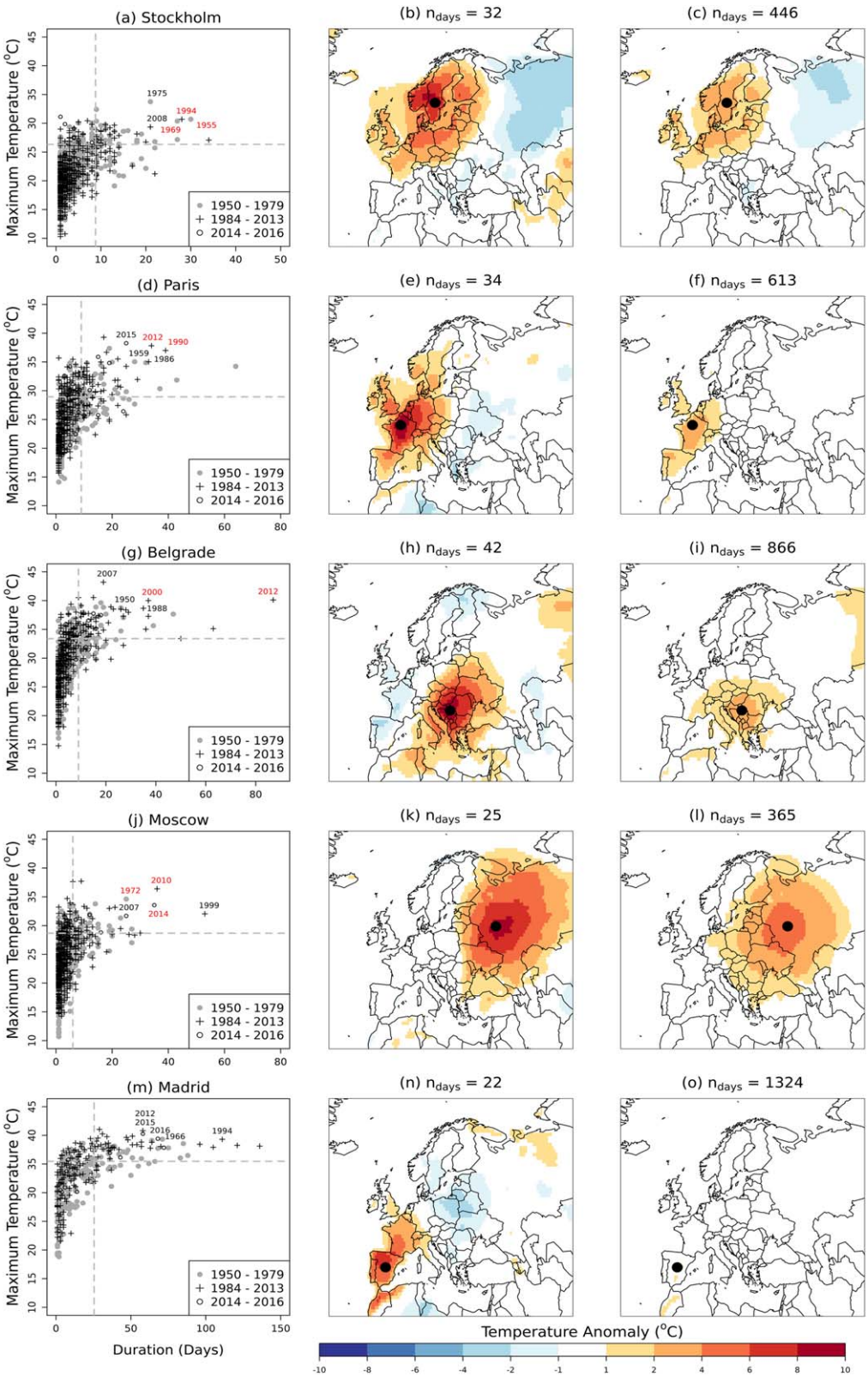

Figure 1. Summary of event characteristics taken from grid points near Stockholm (a)–(c), Paris (d)–(f), Belgrade (g)–(i), Moscow (j)–(l) and Madrid (m)–(o). Panels in the left column provide *xy*-scatter plots of Duration (*D*) and Magnitude (*M*) of events from *ref* (grey dots), *pres* (black crosses) and the period 2014–2016 (black circles). The dashed grey lines represent d_{sel}^{bi} and m_{sel}^{bi} for *D* and *M*, respectively, the bivariate statistical model is fitted to all events that jointly exceed these thresholds in *ref* and *pres* separately. The years are shown next to the points representing top 5 ranked events presented in tables in the appendix, years for events that jointly exceed the 99th percentiles, estimated from *ref* , are shown in red. Panels in the centre column provide temperature anomaly composites considering days on which the maximum temperature was observed during events jointly exceeding d_{sel}^{bi} and m_{sel}^{bi}. Panels in the right column provide temperature composites considering all days during the events jointly exceeding d_{sel}^{bi} and m_{sel}^{bi}. Composites are produced using the ERA Interim dataset.

procedures followed in fitting the statistical models, as well as the methods used in estimating changes in RPs and contributions to changes in bivariate RPs, see appendix A.

3. Results

The joint behaviour of D and M is demonstrated at five grid points near Stockholm, Paris, Belgrade, Moscow and Madrid using xy-scatter plots (figure 1, left column). These illustrate the (D, M) dependence seen throughout Europe where long-duration events generally coincide with high temperatures. Such dependence is explained by the anti-cyclonic conditions underlying DH events, which suppress rainfall and allow for more incoming solar radiation that heats the Earth's surface and atmosphere causing high temperatures to build throughout an event (Miralles *et al* 2014). The top 5 ranked events at each location, from the entire period available (1950–2016), are both provided in tables B1–B5 in appendix B and indicated in figure 1 (left column). Such events have contributed to severe impacts in the affected regions. For example the 2010 event at Moscow was accompanied by extreme heat and wildfires that resulted in 50 000 excess deaths (Shaposhnikov *et al* 2014), while the 1972 event was termed one of the worst modern droughts at the time (Federov 1973, Buchinsky 1976, Schubert *et al* 2014). At Belgrade, the events of 1990 and 2012 brought respective estimated agricultural losses of USD 500 million (Sepulcre-Canto *et al* 2012) and USD 2 billion (Zurovec *et al* 2015). While at Madrid, the 1994 event formed part of Spain's worst 20th century drought event from 1991 to 1995 (Sheffield and Wood 2012) which peaked during the 1994 event according to EDC (2013c). Furthermore the 2012 event led to long-term negative impacts for trees that will have cascading effects on ecosystem services (Camarero *et al* 2015) while the 2015 event covered the hottest July ever recorded in Spain (Ionita *et al* 2017). Further examples are detailed in the appendix which indicate the effectiveness of the characteristics in identifying important events.

The bivariate model, presented in section 2.3, is applied to DH events that reside in the upper right-hand corner defined by the dashed grey lines, representing m^{bi}_{sel} and d^{bi}_{sel}, in figure 1, (left column). Although the characteristics of these events are calculated at a single grid point, they represent anti-cyclonic systems with large spatial extents. To give an idea of their spatial coverage, two types of composite plots of temperature anomalies are produced using ERA Interim data for events in *pres*. A daily temperature anomaly is defined with respect to the climatological mean temperature of all days within a 21 day window centred on the given day. The first composite is produced considering days on which the maximum temperature during an event was observed (figure 1, middle column), while the second is produced considering all days throughout each event (figure 1, right column). The number of days (n_{days}) used to produce the composite is given on each panel.

Stronger anomalies are of course seen for the first type of composite (figure 1, middle column), but both types indicate the affected areas of these events. Within the composites, we also see alternating regions of warm and cold anomalies, particularly in Scandanavia and areas in Central Europe. This feature demonstrates the connection of the event characteristics to blocking systems and sub-tropical ridges, affecting these regions (Sousa *et al* 2018), that are themselves embedded within planetary-scale Rossby waves.

The differences between Madrid and the other locations should be noted. In contrast to the more northern locations, events in Madrid are much longer-lasting and no spatial signature is seen in the composite of temperature anomalies for all event days (figure 1(o)). Thus, in Madrid, unlike the other locations where the characteristics are representative of distinct events, D is most likely representative of a normal summer season while M may represent a single hot event within that season.

3.1. RPs for long-duration and bivariate extreme events

Univariate RPs ($T(d)$) of long-duration dry periods exceeding a duration $d = 15, 20, 30$ and 40 days in *pres* (1984–2013) are presented in figure 2. The spatial distribution of $T(d)$ identifies the differences in synoptic variability seen across Europe during summer. Persistent anti-cyclonic conditions that are common in Southern Europe (Ulbrich *et al* 2012) explain the low values of $T(d)$ seen there, while higher values in more northern parts of Europe are due to a higher synoptic variability between cyclonic and anti-cyclonic conditions.

Bivariate RPs ($T(D_q, M_q)$), computed from *pres*, for joint exceedances of $q =$ 95th and 99th percentiles, respectively, are presented in figure 3. The 95th and 99th percentiles of D and M throughout Europe are provided by figure C1 in appendix C. The (D, M) dependence can influence the estimation of $T(D_q, M_q)$. This influence is quantified using the likelihood multiplication factor (LMF) (Zscheischler and Seneviratne 2017) and is estimated as the ratio between $T(D_q, M_q)$ considering (D, M) dependent (T_{dep}) and independent (T_{ind}) of one another, LMF $= T_{ind}/T_{dep}$ (see appendix for details). The dependence is seen to have a large influence across Europe (figures 3(b) and (d)). For example, treating D and M as independent results in an overestimation of $T(D_{95}, M_{95})$ of up to 8 times the RP when accounting for their dependence.

The spatial distribution of $T(D_{95}, M_{95})$ is mostly homogeneous throughout Western and Eastern Europe (figure 3(a)). The lowest RPs are seen in the Balkans while higher RPs are found in southern areas

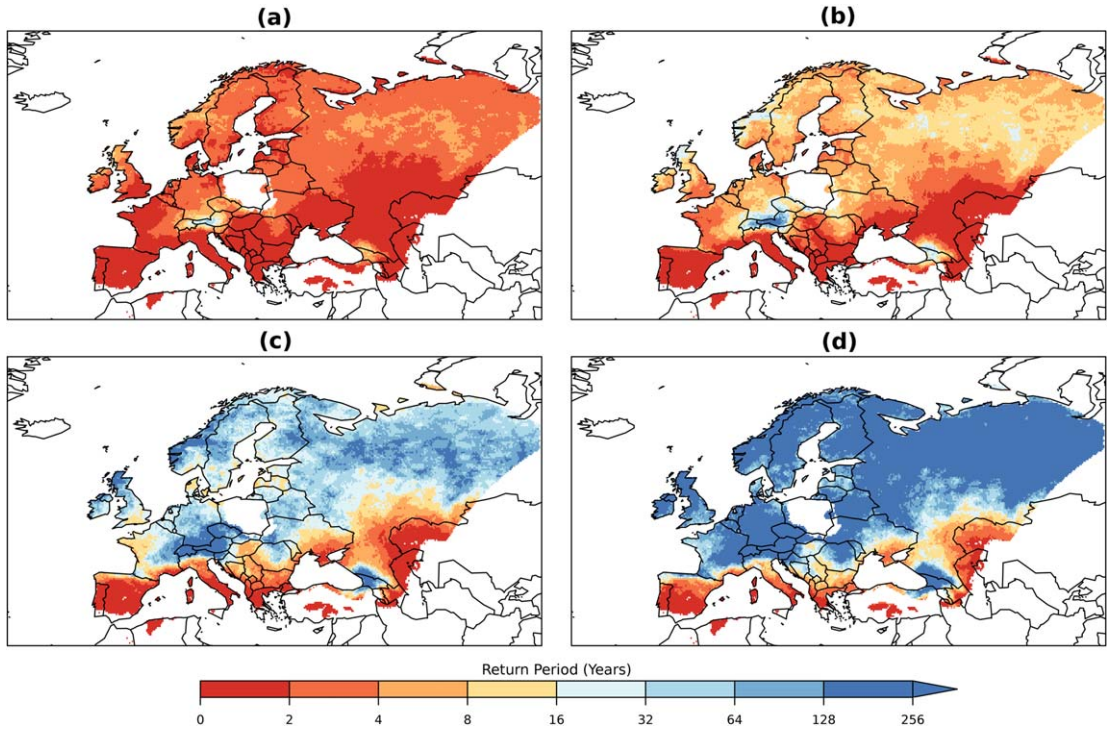

Figure 2. Return periods ($T(d)$) of *DH* events from *pres* (1984–2013) with durations (d) exceeding (a) 15; (b) 20; (c) 30; and (d) 40 d.

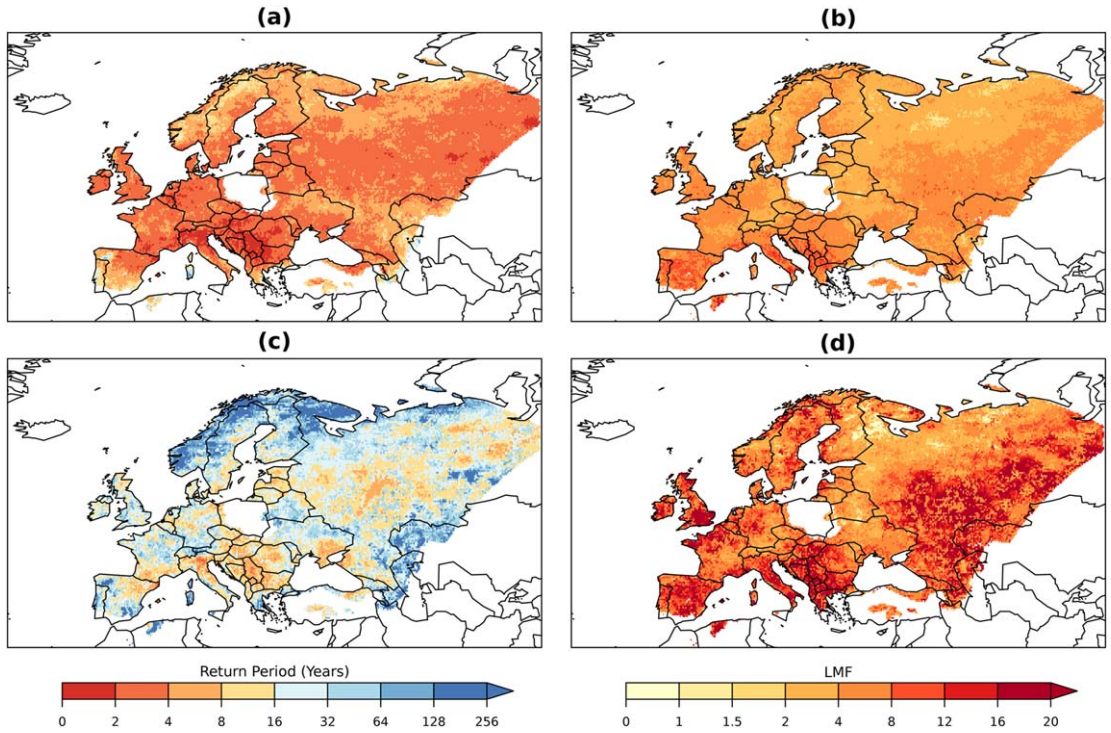

Figure 3. Bivariate return periods of *DH* events from *pres* with joint exceedances of (a) the 95th percentiles ($T(D_{95}, M_{95})$) and (c) 99th percenitles ($T(D_{99}, M_{99})$), along with the likelihood multiplication factor (LMF) that quantifies the influence of the (D, M) dependence on the estimation of (b) $T(D_{95}, M_{95})$ and (d) $T(D_{99}, M_{99})$, a value greater than one signifies that the bivariate return period is overestimated when considering the D and M independent of one another.

such as Spain. The interpretation of $T(D_{95}, M_{95})$ requires careful consideration of both $T(d)$, shown in figure 2, and the local climate. For instance, event characteristics in areas of higher synoptic variability are most likely associated with distinct blocking events or sub-tropical ridges (Sousa *et al* 2018). In areas such as the Balkan region that lie in a transitional climate zone with strong land-atmosphere interactions

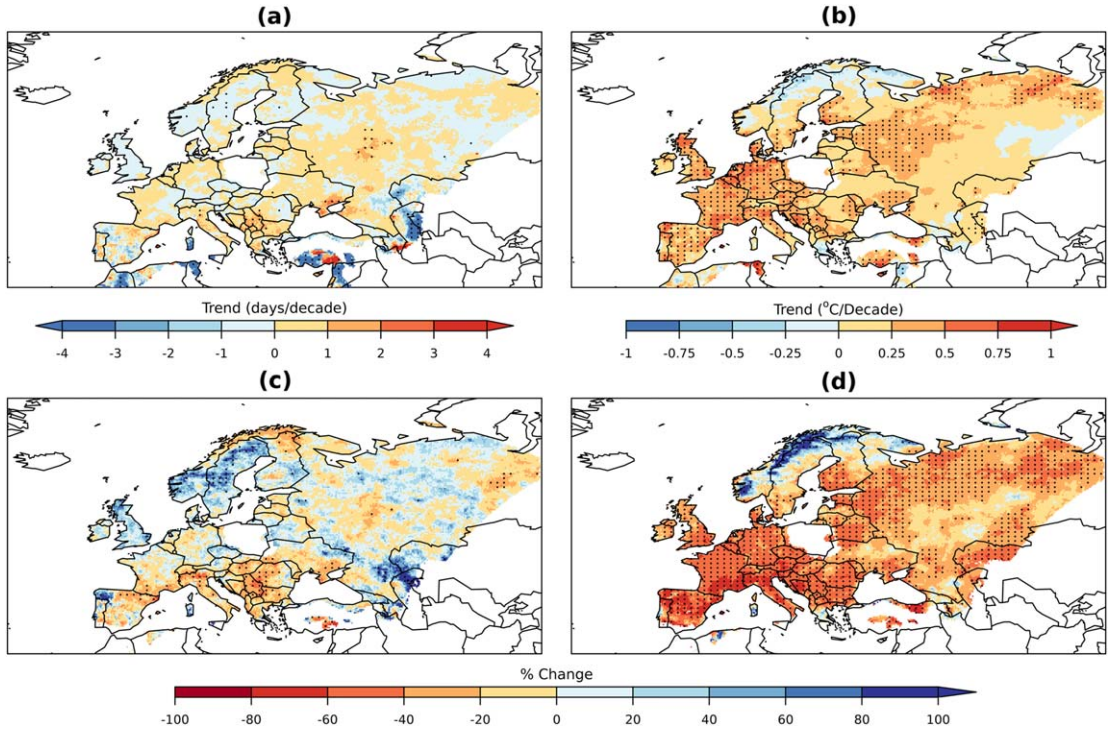

Figure 4. Estimated linear trends in the annual maxima of (a) Duration and (b) Magnitude. Statistically significant trends are indicated by stippling. Also given are the change in univariate RPs in *pres* (1984–2013) with respect to *ref* (1950–1979) of (c) Duration and (d) Magnitude for exceedances of their respective 95th percentiles. Statistically significant differences in the 95% uncertainty interval, estimated via non-parametric bootstrap, are shown by stipling. For all cases, only every 3rd and 5th latitudinal and longitudinal grid point are selected for showing the stippling, showing all points would hide the magnitude of change due to the high resolution of the dataset.

(Hirschi *et al* 2011, Schwingshackl *et al* 2017), drying of soil during a dry period can in turn amplify temperatures (Seneviratne *et al* 2010). This combination may in part explain why the lowest RPs are found in the Balkan region. Meanwhile, in Southern Europe, D can be representative of the normal situation during a large part of the summer season while M may be representative of a single hot event within that season. This results in high values of $T(D_{95}, M_{95})$ due to a smaller number of events that are each very long-lasting.

The occurrence of events with joint exceedances of the 99th percentiles have led to severe impacts in parts of Europe, these events are indicated by the years in red in figure 1. Due to the rare occurrence of such events, the estimation of $T(D_{99}, M_{99})$ is highly sensitive to the occurrence of a single event and as such is subject to large uncertainties. Figure 3(c) provides an indication of where such events have and have not occurred during *pres* and where such events may be more likely to occur again. For example, the areas of 2010 and 2012 events in Russia and South-East Europe are highlighted by lower values of $T(D_{99}, M_{99})$ (figure 3(c)). However, it does not provide robust information of locations where such extreme events are unlikely to occur. This is emphasised by the recent record breaking 2018 dry and hot period that had severe impacts in much of Northern Europe, where large RPs are found (figure 3(c)). Robust estimates of the probability of such rare events are not obtainable using empirical data, particularly with non-stationarities imposed by a changing climate. Such estimates require ensembles of suitable climate models that provide a larger sample of events and perhaps more creative methods to understand the changing probability and future likelihood of such rare events (Hazeleger *et al* 2015, Bevacqua *et al* 2017). For these reasons, we present the analysis of changes to $T(D_{95}, M_{95})$ in the next sections as we have greater confidence in its estimation.

3.2. Variations in duration and magnitude

Figure 4 presents the linear trends, estimated via linear regression, in the annual maxima of D and M over the entire observation period (1950–2013), as well as the percentage change between *ref* and *pres* in $T(D_{95})$ and $T(M_{95})$ estimated via equation (A.2) (see appendix A for details).

Between D and M, the strongest relative changes in both the annual maxima and 95th percentile exceedances are seen for M across Europe. Positive linear trends are seen in the annual maxima of M in much of Western Europe and parts of Eastern Europe (figure 4(b)). These trends can be between 0.25 °C and 0.5 °C per decade, meaning that the annual maximum of M in DH events may have warmed by 1.5 °C–3 °C over the 64 year observation period. Large differences

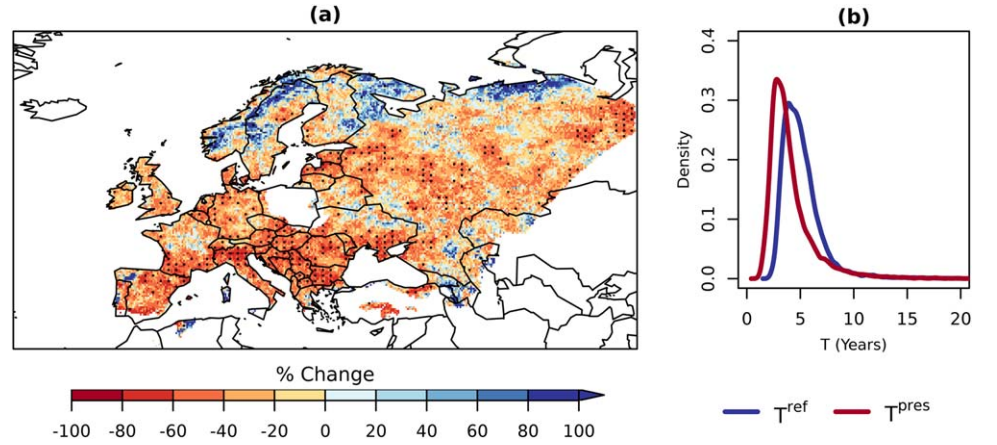

Figure 5. Estimated change in bivariate RPs in *pres* (1984–2013) with respect to *ref* (1950–1979) for joint exceedances of their respective 95th percentiles. Shown in (a) are the % changes across Europe, stippling indicates statistically significant differences between *pres* and the 95% uncertainty interval from *ref* estimated via non-parametric bootstrap. Only every 3rd and 5th latitudinal and longitudinal grid point are selected for showing the stippling. Alongside in (b) are the kernel densities estimated using the RPs from all grid points for *ref* (blue) and *pres* (red).

in $T(M_{95})$ between *ref* and *pres* are found across Europe (figure 4(d)). The frequency of exceedances has almost doubled in many locations though much of Northern Scandinavia has seen a halving in frequency, which is in contrast to changes in the seasonal mean (see figure C2 in appendix C). The physical reasoning for different behaviours between the mean and extremes is unclear. It may involve changes in atmospheric circulation that are largely dominated by natural variability (Woollings *et al* 2018) and/or changes in soil moisture from permafrost melting due to increased seasonal mean temperatures (see figure C2 in appendices). The latter may lead to an increase in both the moisture availability in soil and evapotranspiration during summer (Lawrence *et al* 2015) which may in turn dampen temperature extremes through latent cooling.

Weak variations are observed for D. Significant trends in the annual maximum duration are found only in a particular region of Russia and South-Eastern Europe (figure 4(a)). These trends can be between 1 and 2 days per decade such that the annual maximum duration may have increased by between 6 and 12 days over the 64 years in these locations. Variations in D_{95} are also mostly small. The strongest increases are found in South-Eastern Europe and parts of Russia while the strongest decreases are seen across much of the UK, Scandinavia and Russia.

3.3. Variations in bivariate RPs

The change in $T^{pres}(D_{95}, M_{95})$ with respect to $T^{ref}(D_{95}, M_{95})$, estimated via equation (A.2) (see appendix A), is provided in figure 5(a). Statistically significant differences between *pres* and *ref*, indicated by the stippling in figure 5(a), are identified when $T^{pres}(D_{95}, M_{95})$ is outside the 95% uncertainty interval of $T^{ref}(D_{95}, M_{95})$. The strongest changes are seen just north of the Mediterranean, particularly in South-Eastern Europe, and across much of Western Russia. Statistically significant negative changes (increased probability) are found throughout these regions and cover 17% of the total area of the dataset. Figure 5(b) presents the kernel density estimates of $T^{ref}(D_{95}, M_{95})$ and $T^{pres}(D_{95}, M_{95})$ from each grid point throughout Europe. Comparing these highlights the general shift across Europe to lower bivariate RPs and thus a higher frequency of *DH* events during *pres* compared to *ref*.

These changes in $T(D_{95}, M_{95})$, shown in figure 5, can arise due to changes in the marginal distributions of (a) D and (b) M as well as due to changes in (c) the (D, M) dependence. Using methods outlined in appendix A.4, we decompose the changes in bivariate RPs to quantify the contribution of these three components to the variation in $T(D_{95}, M_{95})$. Changes in marginal density of M have the largest contributions as indicated by the higher amount of stippling (figure 6(b)), while changes in D are seen to have a contribution in some areas of Europe (figure 6(a)), most specifically in the Balkans where the largest changes in D are seen (figure 4(a)). Large contributions are also seen from variations in the (D, M) dependence (figure 6(c)) owing to an increase in the dependence between D and M. The physical reasoning behind this increase is unclear and as there are very few significant changes, it is likely that contributions from variations in dependence are dominated by a single event such as the 2010 Russian heat wave. In fact, some of the areas showing the largest contribution from changes in dependence correspond to the area affected by the Russian heat wave in 2010.

Overall, with large variations in M and only small variations found in D, the results illustrate the predominant influence of temperature on the increased frequency of *DH* events seen across Europe as there is little evidence to suggest that events are more prolonged in *pres*. Thus, *DH* events are, in general, becoming warmer but not longer.

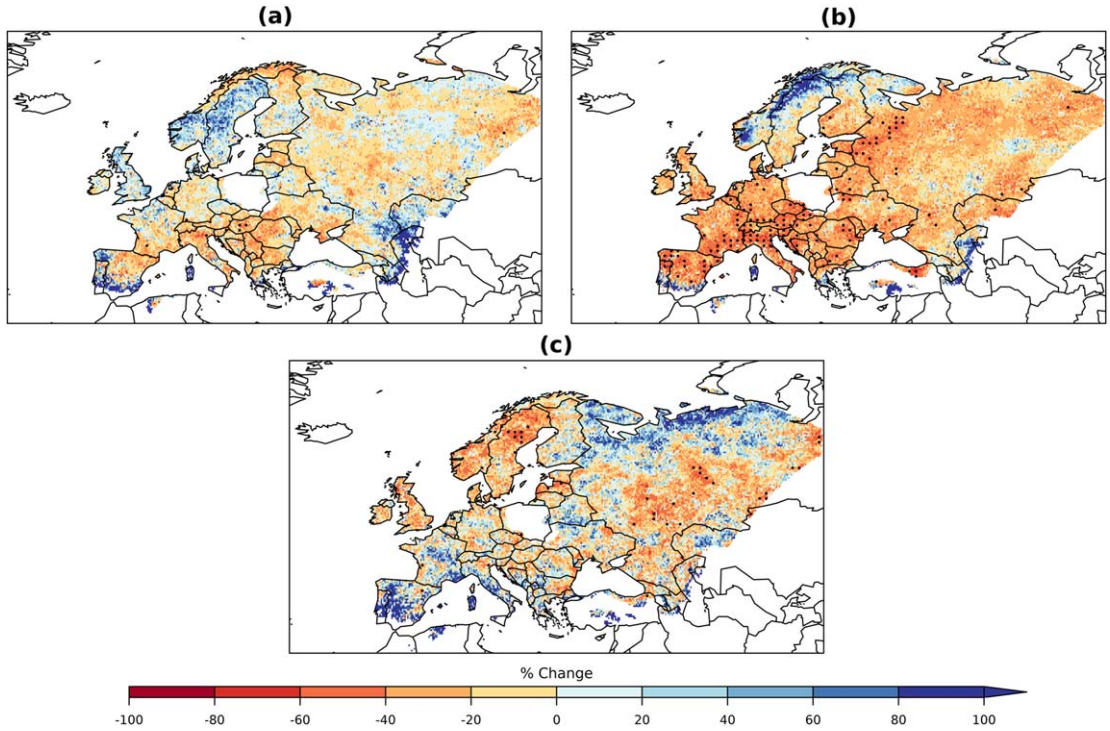

Figure 6. Contributions to changes in bivariate RPs between *ref* and *pref* from changes in the marginal densities of (a) Duration, and (b) Magnitude, as well as from changes in (c) dependence. Statistically significant differences between T_{exp_i} and T^{ref} are indicated by stippling. Only every 3rd and 5th latitudinal and longitudinal grid point are selected for showing the stippling.

4. Summary and conclusions

We have investigated long-duration dry events that co-occur with extreme temperatures in Europe, as well as changes in these events over the period 1950–2013. This paper proposes a framework to characterise such events and quantify their probability and RPs through the application of a copula-based approach introduced by Bevacqua *et al* (2018). The events are denoted as long-duration dry and hot (*DH*) events and are characterised by their duration *D* (consecutive number of day with precipitation less than 1mm), and magnitude *M* (maximum daily maximum temperature during event). These characteristics combined are shown here to be effective in highlighting important events that have brought severe impacts to affected regions.

The probability of such compound events, with respect to joint exceedances of the respective 95th percentiles of *D* and *M*, has increased across much of Europe between *ref* (1950–1979) and *pres* (1984–2013) periods. The main driver of this change in probability is increasing temperatures throughout Europe. Little change is seen in the duration of events, leading us to conclude that *DH* events have mostly become warmer during *pres* rather than longer. An exception to this is found in South-East Europe where events appear to have increased in temperature and duration.

RPs were also estimated for events in which *D* and *M* jointly exceed their 99th percentiles. However, robust estimations of their probability are not possible to obtain due to the rarity of their occurrence. For this reason, we cannot assess changes in these RPs. Such events have brought severe impacts to the affected regions and so it is important that efforts are made to better quantify their probability such that possible future changes in their occurrence may be better understood (Coumou *et al* 2018). It is hoped that the methodology used in characterising these events and quantifying their probability will provide a platform for further research, particularly in extracting information of their current and future probability from climate models.

The implications of the increased probability of *DH* events found here mainly pertain to the acceleration of drought propagation from meteorological drought to soil moisture drought. The results complement other findings with respect to the relationship between drought and climate change. For example, soil moisture drought events are expected to set in quicker and become more severe (Trenberth *et al* 2014, Samaniego *et al* 2018), owing to increases in evaporation during dry periods (Dai *et al* 2004) that are driven by rising temperatures (Scheff and Frierson 2014, Zhao and Dai 2015). Furthermore, given the weak historical trends found in global land precipitation (New *et al* 2001, Lambert *et al* 2004, Ren *et al* 2013, Adler *et al* 2017), the dominant temperature signal behind the increased probability of DH events may also largely explain changes in global drought conditions, as shown in Marvel *et al* (2019), which closely resemble changes in global mean temperature (e.g.

Pachuari *et al* (2014)). The results may also have implications for the persistence of soil moisture drought conditions. High amounts of precipitation are required for recovery from large moisture deficits induced by intense drying (Seneviratne *et al* 2012, Manning *et al* 2018) while general increases in evaporation can push environments towards a climatically drier state (Samaniego *et al* 2018).

The response of D and M to climate change can also be linked to that of blocking events. The weak variations seen in D align with studies on changes in blocking frequency which is expected to be dominated by natural variability in the coming decades (Woollings *et al* 2018). Consistent with the changes in M shown here, blocking events have become warmer and are expected to become more extreme in the future (Sousa *et al* 2018) due to increasing temperatures and decreasing soil moisture that can strengthen temperature extremes through land-atmosphere interactions (Seneviratne *et al* 2006).

One should note that these results are derived from a gridded dataset which may introduce errors through interpolation of station observations whose spatial density can be too low for adequate representation of extremes (Haylock *et al* 2008, Herrera *et al* 2018). Although we have more confidence in this dataset for large-scale events investigated here than for localised precipitation extremes, as investigated in (Herrera *et al* 2018) for instance, it would be interesting to investigate the influence of interpolation and the spatial density of stations on the representation of characteristics of *DH* events in gridded products. This would provide important information for climate model validation studies that incorporate EOBS and other gridded datasets.

Finally, the comparison made here between *ref* and *pres* shows differences in the multi-decadal variability of *DH* events. Direct attribution of these events to anthropogenic climate change is not possible with an empirical analysis. However, our finding that temperature changes are the main cause for changes in bivariate probability is in line with trends of increasing temperature due to rising greenhouse gas concentrations. One can therefore hypothesise, alongside forewarnings from Samaniego *et al* (2018), that such increases in probability will continue into the future leading to more severe long-lasting soil moisture droughts that can lead to negative impacts such as reduced crop yields and increased wildfire risk.

Acknowledgments

Colin Manning received funding from the CE:LLO project funded by the Volkswagen Foundation (Az.: 88469), which also supported project meetings. The authors would like to sincerely thank the two anonymous reviewers whose comments and questions led to the improvement of this manuscript.

Appendix A. Methods appendix

A.1. Statistical models selection

Univariate stationary parametric models are fitted to exceedances of the thresholds d_{sel}^{uni} and m_{sel}^{uni} (*sel*: selected, *uni*: univariate) for D and M respectively. The default selection for each threshold is the 90th percentile of the given variable, estimated from the *ref* period (1950–1979), though this is decreased in cases where there are not at least 20 events, but never below the 70th percentile from *ref* . Grid points with fewer than 20 events exceeding the 70th percentile are removed from the analysis. These cases are found in arid regions such as Southern Spain, Turkey and Northern Africa where dry events are generally very long lasting, resulting in very few events. Similarly, the parametric copula-based probability distribution is fitted to events in which D and M jointly exceed their respective thresholds d_{sel}^{bi} and m_{sel}^{bi} (*sel*: selected, *bi*: bivariate). Again the default selection for each threshold is the 90th percentile from *ref* and both are simultaneously decreased if there is not at least 20 events, but never below their 70th percentiles.

Duration exceedances of the thresholds d_{sel}^{uni} and d_{sel}^{bi} are modelled using an exponential distribution. A geometric distribution is generally used for D but the application of copulas requires continuous marginals, and so we employ its continuous counterpart as done in Serinaldi *et al* (2009). Magnitude exceedances of m_{sel}^{uni} and m_{sel}^{bi} are modelled using the Generalised Pareto Distribution. Copulas were fitted to u_D and u_M. These were obtained via empirical marginal CDF in order to avoid errors introduced by potential misspecification of the parameters of the marginal distributions.

The copula family was selected at each grid point separately from the highest ranked of the following families according to the akaike information criterion (AIC): Gaussian, t, Clayton, Gumbel, Frank, Joe, BB1, BB6, BB7, and BB8. At some grid points, we find a negative dependence between pairs that jointly exceed d_{sel}^{bi} and m_{sel}^{bi}. For these cases we fit an independent copula as the overall dependence between D and M is always positive such that a negative dependence between joint exceedances is likely unphysical and due to the small number of data points. The selected copulas are shown in figure C3 in appendix C. By selecting from a range of copula, we choose the best model according to the AIC at each grid point. Alternatively, one could select an optimal copula for all grid points, as is the case for marginal distributions. However, we choose not to do this as we do not have prior knowledge of the true structure of dependence and have too few data to gain such knowledge. Applying a single

copula would also assume a homogeneous dependence structure exists across Europe. This assumption may not be reasonable and can reduce the quality of fit regionally and locally (not shown).

Marginal distributions and copulas were fitted through a maximum likelihood estimator using the fitdistrplus (Delignette-Muller and Dutang 2015), ismev (Heffernan and Stephenson 2018) and VineCopula (Schepsmeier *et al* 2017) R packages. The goodness of fit of marginals and copulas (one-tailed; $N_{boot} = 100$ for copulas) was tested using the CvM criterion with the goftest (Faraway *et al* 2017), eva (Bader and Yan 2018) and VineCopula R packages. The selected distribution or copula family is rejected if the p-value is less than 0.05. This occurs at less than 5% of grid points for each case, which is in the acceptable range of tests that may fail by random chance (Zscheischler *et al* 2017).

A.2. Influence of dependence of bivariate RP estimation

The (D, M) dependence can influence the estimation of the bivariate RP $T(D_q, M_q)$. We quantify this influence using the LMF (Zscheischler and Seneviratne 2017), which is estimated as the ratio between $T(D_q, M_q)$ considering (D, M) dependent (T_{dep}) and independent (T_{ind}) of one another:

$$\mathrm{LMF} = T_{ind}/T_{dep} \tag{A.1}$$

T_{dep} is estimated using equation (3), while T_{ind} is computed considering D and M independent of one another. In this case, an independent copula is chosen for C and $\mu_E = N_Y/N_{ind}$, where N_{ind} is the expected number of joint exceedances for two independent variables (the total number of events (including non-extremes) multiplied by the probability of a joint exceedance above q in the independent case). F_D and F_M are then fitted to all marginal exceedances of the thresholds d_{sel}^{uni} and m_{sel}^{uni}.

A.3. Estimation of annual trends and RP variation

Linear trends are estimated for the annual maxima of D and M from DH events throughout the entire analysis period (1950–2013) using linear regression. We use a significance level of $p = 0.05$ to identify statistically significant trends.

We estimate changes in the RP for individual and joint exceedances of the 95th percentiles of D and M. The analysis period is split into two 30 year periods, a reference (*ref* : 1950–1979) and present period (*pres*: 1984–2013), and RPs are estimated in each period separately, while the 95th percentiles are estimated from *ref*. The change in case $i =$ (a) $T(D_{95})$, (b) $T(M_{95})$, and (c) $T(D_{95}, M_{95})$, is calculated in *pres* with respect to *ref* as:

$$\Delta T_i = \frac{T_i^{pres} - T_i^{ref}}{T_i^{ref}} \cdot 100, \tag{A.2}$$

where ΔT_i refers to the change of RP in *pres* (T_i^{pres}) with respect to that estimated in *ref* (T_i^{ref}). The statistical significance of changes is identified through comparing T_i^{pres} with the 95% uncertainty interval surrounding T_i^{ref}. This uncertainty interval is constructed, via non-parametric bootstrapping, from 1000 values of T_i^{ref} obtained from 1000 event sets. These are created by resampling of the entire distribution such that we consider the uncertainties around μ_i also.

A.4. Contributions to RP variation

Using a method developed in Bevacqua *et al* (2018), we assess the relative contributions to changes in bivariate RPs arising from changes in the marginal distributions of (a) D, (b) M, and (c) the (D, M) dependence. The relative change in probability for each case is estimated as:

$$\Delta T_{exp_i} = \frac{T_{exp_i} - T^{ref}}{T^{ref}} \cdot 100, \tag{A.3}$$

where T^{ref} is the bivariate RP from *ref* while T_{exp_i} is calculated in the following manner:

Experiment (a): Given the variable D^{ref}, we calculate the associated empirical CDF to obtain $U_{D^{ref}}$. From the variable D^{pres} we define the empirical CDF $F_{D^{pres}}$ that is used to obtain $D_a = F^{-1}_{D^{pres}}(U_{D^{ref}})$. We then compute the RP T_{exp_a} using the bivariate model fitted to (D_a, M^{ref}) pairs that jointly exceed d_{sel}^{bi} and m_{sel}^{bi}. The variables (D_a, M^{ref}) have the same Spearman correlations and tail dependence as during *ref* but the marginal distribution of D is that of *pres*.

Experiment (b): Similar to Experiment (a) but swapping D and M.

Experiment (c): With variables (D^{ref}, M^{ref}) we obtain their respective empirical CDFs from which we define $D_c = F^{-1}_{D^{ref}}(U_{D^{pres}})$ and $M_c = F^{-1}_{M^{ref}}(U_{M^{pres}})$. The variables ($D_c$, M_c) have the same Spearman correlation and tail dependence as (D^{pres}, M^{pres}), but the marginal distributions are those of *ref* . The RP T_{exp_c} is then computed using the bivariate model fitted to (D_c, M_c) pairs jointly exceeding d_{sel}^{bi} and m_{sel}^{bi}.

Appendix B. Additional tables appendix: top 5 events at selected locations

Table B1. Top 5 Events from Stockholm grid cell. The top 5 events at each site are selected based on a combined ranking, r_{DM}, based on a sum of the individual ranks of duration (r_D) and magnitude r_M, i.e. $r_{DM} = r_D + r_M$. The event with the highest combined ranking will be that with the largest r_{DM} value.

D (days)	M (°C)	Start date	References
30	30.70	06 July 1955	Veryard (1956)
28	30.69	30 June 1994	Stagge *et al* (2013)
21	33.75	25 July 1975	SPCCA (2016)
27	30.38	25 July 1969	Hannaford *et al* (2011)
21	29.36	20 May 2008	No Information

Table B2. Top 5 Events from Paris grid cell. Events ranked as described in the caption of table B1.

D (days)	M (°C)	Start date	References
39	37.00	06 July 1990	Stagge *et al* (2013)
34	37.82	06 August 2012	No Information
25	38.26	23 June 2015	Ionita *et al* (2017)
33	35.03	07 July 1986	No Information
28	35.04	01 July 1959	Stagge *et al* (2013)

Table B3. Top 5 Events from Belgrade grid cell. Events ranked as described in the caption of table B1.

D (days)	M (°C)	Start date	References
87	40.12	30 July 2012	Zurovec *et al* (2015)
37	40.00	21 July 2000	Sepulcre-Canto *et al* (2012)
35	38.67	17 July 1988	No Information
26	38.74	06 August 1950	Tošić and Unkašević (2014)
19	43.20	12 July 2007	Sepulcre-Canto *et al* (2012)

Table B4. Top 5 Events from Moscow grid cell. Events ranked as described in the caption of table B1.

D (days)	M (°C)	Start date	References
36	36.40	17 June 2010	Mokhov (2011)
25	34.61	29 July 1972	Schubert *et al* (2014)
35	33.56	03 July 2014	Russo *et al* (2015)
53	32.04	01 June 1999	Schubert *et al* (2014)
21	33.18	08 August 2007	Schubert *et al* (2014)

Table B5. Top 5 Events from Madrid grid cell. Events ranked as described in the caption of table B1.

D (days)	M (°C)	Start date	References
111	39.31	02 June 1994	Stagge *et al* (2013)
58	40.83	27 July 2012	Camarero *et al* (2015)
71	39.33	03 July 1966	Cantos *et al* (2000)
58	40.28	24 June 2015	Ionita *et al* (2017)
68	39.41	07 July 2016	Vázquez *et al* (2016)

Appendix C. Additional figures appendix

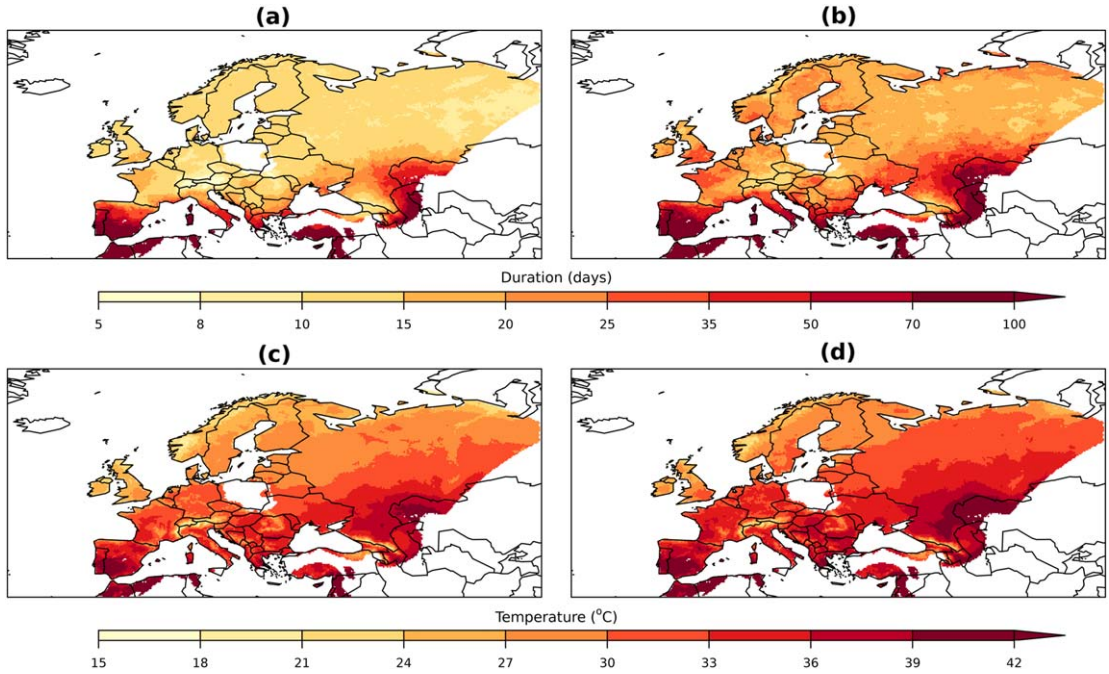

Figure C1. Absolute values at the 95th and 99th percentiles throughout Europe for *D* ((a) and (c)) and *M* ((b) and (d)).

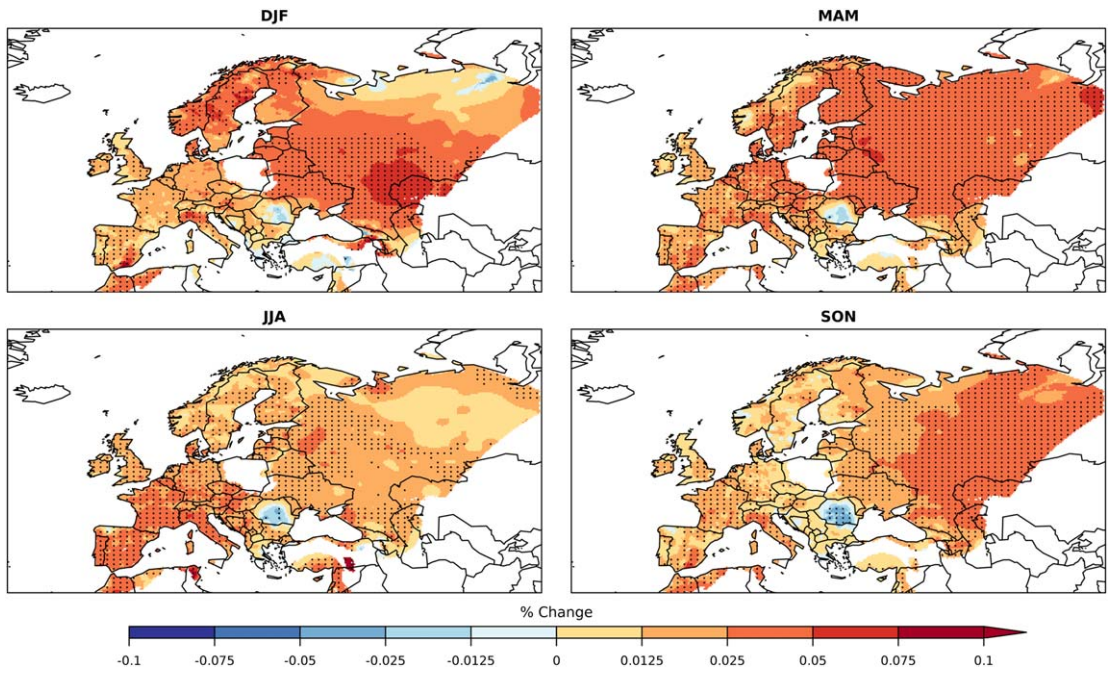

Figure C2. Estimated linear trends in the seasonal mean of temperature for winter (DJF), spring (MAM), summer (JJA) and autumn (SON) over the historical period 1950–2013. Statistically significant trends are indicated by stippling.

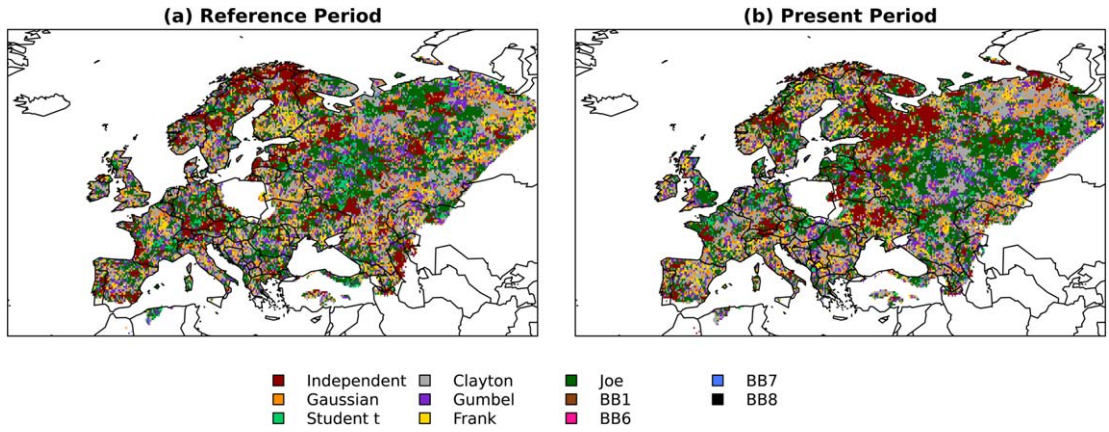

Figure C3. Selected copula families for (a) *ref* (1950–1979), and (b) *pres* (1984–2013) periods.

ORCID iDs

Colin Manning https://orcid.org/0000-0001-5364-3569
Martin Widmann https://orcid.org/0000-0001-5447-5763
Emanuele Bevacqua https://orcid.org/0000-0003-0472-5183
Anne F Van Loon https://orcid.org/0000-0003-2308-0392
Douglas Maraun https://orcid.org/0000-0002-4076-0456

References

Adler R F, Gu G, Sapiano M, Wang J-J and Huffman G J 2017 Global precipitation: means, variations and trends during the satellite era (1979–2014) *Surv. Geophys.* **38** 679–99

AghaKouchak A, Cheng L, Mazdiyasni O and Farahmand A 2014 Global warming and changes in risk of concurrent climate extremes: insights from the 2014 California drought *Geophys. Res. Lett.* **41** 2014GL062308

Bader B and Yan J 2018 Eva: extreme value analysis with goodness-of-fit testing (Computer software manual)

Bevacqua E, Maraun D, HobæHaff I, Widmann M and Vrac M 2017 Multivariate statistical modelling of compound events via pair-copula constructions: analysis of floods in Ravenna (Italy) *Hydrol. Earth Syst. Sci.* **21** 2701–23

Bevacqua E, Maraun D, Vousdoukas M I, Voukouvalas E, Vrac M, Mentaschi L and Widmann M 2018 Higher probability of compound flooding from precipitation and storm surge in Europe under anthropogenic climate change *Science Advances* (https://doi.org/10.31223/osf.io/ta764)

Buchinsky I E 1976 Droughts and dry winds (in Russian) *Gidrometeoizdat* 214

Camarero J J, Gazol A, Sangüesa-Barreda G, Oliva J and Vicente-Serrano S M 2015 To die or not to die: early warnings of tree dieback in response to a severe drought *J. Ecol.* **103** 44–57

Cantos J O, Gil A M and Amorós A M R 2000 Diferentes percepciones de la sequía en España: adaptación, catastrofismo e intentos de corrección *Investigaciones Geográficas* **23** 5–46

Ciais P *et al* 2005 Europe-wide reduction in primary productivity caused by the heat and drought in 2003 *Nature* **437** 529–33

Coles S, Bawa J, Trenner L and Dorazio P 2001 *An Introduction to Statistical Modeling of Extreme Values* vol 208 (Berlin: Springer)

Coumou D, Di Capua G, Vavrus S, Wang L and Wang S 2018 The influence of Arctic amplification on mid-latitude summer circulation *Nat. Commun.* **9** 2959

Dai A 2013 Increasing drought under global warming in observations and models *Nat. Clim. Change* **3** 52–8

Dai A, Trenberth K E and Qian T 2004 A global dataset of palmer drought severity index for 1870–2002: relationship with soil moisture and effects of surface warming *J. Hydrometeorol.* **5** 1117–30

Dee D P *et al* 2011 The ERA-Interim reanalysis: configuration and performance of the data assimilation system *Q. J. R. Meteorol. Soc.* **137** 553–97

Delignette-Muller M L and Dutang C 2015 Fitdistrplus: an R package for fitting distributions *J. Stat. Softw.* **64** 1–34

Donat M *et al* 2013 Updated analyses of temperature and precipitation extreme indices since the beginning of the twentieth century: the HadEX2 dataset *J. Geophys. Res.: Atmos.* **118** 2098–118

Dorigo W *et al* 2011 The international soil moisture network: a data hosting facility for global *in situ* soil moisture measurements *Hydrol. Earth Syst. Sci.* **15** 1675–98

EDC 2013a *Drought of 1959* (http://geo.uio.no/edc/droughtdb/edr/DroughtEvents/1959 Event.php)

EDC 2013b *Drought of 1989–1990* (http://geo.uio.no/edc/droughtdb/edr/DroughtEvents/ 1989 Event.php)

EDC 2013c *Drought of 1991–1995* (http://geo.uio.no/edc/droughtdb/edr/DroughtEvents/_1991_Event.php)

Faraway J, Marsaglia G, Marsaglia J and Baddeley A 2017 Goftest: Classical goodness-of-fit tests for univariate distributions (Computer software manual) (https://CRAN.R-project.org/package=goftest) (R package version 1.1-1)

Federov E K 1973 Weather and yield (in Russian) *Gidrometeoizdat* 55

Fleig A K, Tallaksen L M, Hisdal H and Demuth S 2006 A global evaluation of streamflow drought characteristics *Hydrol. Earth Syst. Sci.* **10** 535–52

Gudmundsson L, Rego F, Rocha M and Seneviratne S I 2014 Predicting above normal wildfire activity in southern europe as a function of meteorological drought *Environ. Res. Lett.* **9** 084008

Gudmundsson L and Seneviratne S I 2016 Anthropogenic climate change affects meteorological drought risk in Europe *Environ. Res. Lett.* **11** 044005

Hannaford J, Lloyd-Hughes B, Keef C, Parry S and Prudhomme C 2011 Examining the large-scale spatial coherence of European drought using regional indicators of precipitation and streamflow deficit *Hydrol. Process.* **25** 1146–62

Haylock M, Hofstra N, Tank A K, Klok E, Jones P and New M 2008 A European daily high-resolution gridded data set of surface temperature and precipitation for 1950–2006 *J. Geophys. Res.: Atmos.* **113**

Hazeleger W *et al* 2015 Tales of future weather *Nat. Clim. Change* **5** 107

Heffernan J E and Stephenson A G 2018 Ismev: An introduction to statistical modeling of extreme values (Computer software manual) (https://CRAN.R-project.org/package=ismev) (R package version 1.42)
Hegerl G C, Hanlon H and Beierkuhnlein C 2011 Climate science: elusive extremes *Nat. Geosci.* **4** 142–3
Herrera S, Kotlarski S, Soares P M, Cardoso R M, Jaczewski A, Gutiérrez J M and Maraun D 2018 Uncertainty in gridded precipitation products: influence of station density, interpolation method and grid resolution *Int. J. Climatol.* (https://doi.org/10.1002/joc.5878)
Hirschi M *et al* 2011 Observational evidence for soil-moisture impact on hot extremes in southeastern Europe *Nat. Geosci.* **4** 17–21
Ionita M, Tallaksen L, Kingston D, Stagge J, Laaha G, Van Lanen H, Scholz P, Chelcea S and Haslinger K 2017 The European 2015 drought from a climatological perspective *Hydrol. Earth Syst. Sci.* **21** 1397–419
Lambert F H, Stott P A, Allen M R and Palmer M A 2004 Detection and attribution of changes in 20th century land precipitation *Geophys. Res. Lett.* **31**
Lawrence D M, Koven C, Swenson S C, Riley W and Slater A 2015 Permafrost thaw and resulting soil moisture changes regulate projected high-latitude co_2 and ch_4 emissions *Environ. Res. Lett.* **10** 094011
Lehtonen I, Ruosteenoja K and Jylhä K 2014 Projected changes in european extreme precipitation indices on the basis of global and regional climate model ensembles *Int. J. Climatol.* **34** 1208–22
Manning C, Widmann M, Bevacqua E, Van Loon A F, Maraun D and Vrac M 2018 Soil moisture drought in Europe: a compound event of precipitation and potential evapotranspiration on multiple time scales *J. Hydrometeorol.* **19** 1255–71
Marvel K, Cook B I, Bonfils C J, Durack P J, Smerdon J E and Williams A P 2019 Twentieth-century hydroclimate changes consistent with human influence *Nature* **569** 59
Mazdiyasni O and AghaKouchak A 2015 Substantial increase in concurrent droughts and heatwaves in the United States *Proc. Natl Acad. Sci.* **112** 11484–9
Miralles D G, Teuling A J, Van Heerwaarden C C and De Arellano J V-G 2014 Mega-heatwave temperatures due to combined soil desiccation and atmospheric heat accumulation *Nat. Geosci.* **7** 345–9
Mitchell K E *et al* 2004 The multi-institution North American land data assimilation system (nldas): utilizing multiple GCIP products and partners in a continental distributed hydrological modeling system *J. Geophys. Res.: Atmos.* **109**
Mokhov I 2011 Specific features of the 2010 summer heat formation in the European territory of Russia in the context of general climate changes and climate anomalies *Izv., Atmos. Ocean. Phys.* **47** 653–60
New M, Todd M, Hulme M and Jones P 2001 Precipitation measurements and trends in the twentieth century *Int. J. Climatol.* **21** 1889–922
Orlowsky B and Seneviratne S I 2012 Global changes in extreme events: regional and seasonal dimension *Clim. Change* **110** 669–96
Pachuari R K, Allen M R, Barros V R, Broome J, Cramer W, Christ R, Church J A, Clarke L, Dahe Q and Dasgupta P 2014 Contribution of working groups I, II and III to the fifth assessment report of the Intergovernmental Panel on Climate Change *Climate Change 2014: Synthesis Report* (Geneva, Switzerland: IPCC)
Ren L, Arkin P, Smith T and Shen S P 2013 Global precipitation trends in 1900–2005 from a reconstruction and coupled model simulations *J. Geophys. Res. Atmos.* **118** 1679–89
Robock A *et al* 2000 The global soil moisture data bank *Bull. Am. Meteorol. Soc.* **81** 1281–300
Ruffault J, Moron V, Trigo R and Curt T 2016 Objective identification of multiple large fire climatologies: an application to a Mediterranean ecosystem *Environ. Res. Lett.* **11** 075006
Russo S, Sillmann J and Fischer E M 2015 Top ten European heatwaves since 1950 and their occurrence in the coming decades *Environ. Res. Lett.* **10** 124003
Salvadori G, De Michele C, Kottegoda N T and Rosso R 2007 *Extremes in Nature: An Approach Using Copulas* vol 56 (Berlin: Springer)
Samaniego L *et al* 2018 Anthropogenic warming exacerbates european soil moisture droughts *Nat. Clim. Change* **8** 421
Scheff J and Frierson D M 2014 Scaling potential evapotranspiration with greenhouse warming *J. Clim.* **27** 1539–58
Schepsmeier U, Stoeber J, Brechmann E C, Graeler B, Nagler T and Erhardt T 2017 Vinecopula: statistical inference of vine copulas (Computer software manual) (http://CRAN.R-project.org/package=VineCopula) (R package version 2.1.1)
Schubert S D, Wang H, Koster R D, Suarez M J and Groisman P Y 2014 Northern Eurasian heat waves and droughts *J. Clim.* **27** 3169–207
Schwingshackl C, Hirschi M and Seneviratne S I 2017 Quantifying spatiotemporal variations of soil moisture control on surface energy balance and near-surface air temperature *J. Clim.* **30** 7105–24
Seneviratne S I 2012 Climate science: historical drought trends revisited *Nature* **491** 338–9
Seneviratne S I *et al* 2010 Investigating soil moisture-climate interactions in a changing climate: a review *Earth Sci. Rev.* **99** 125–61
Seneviratne S I *et al* 2012 Swiss prealpine Rietholzbach research catchment and lysimeter: 32 year time series and 2003 drought event *Water Resour. Res.* **48** W06526
Seneviratne S I, Lüthi D, Litschi M and Schär C 2006 Land-atmosphere coupling and climate change in Europe *Nature* **443** 205–9
Sepulcre-Canto G, Horion S, Singleton A, Carrao H and Vogt J 2012 Development of a combined drought indicator to detect agricultural drought in Europe *Nat. Hazards Earth Syst. Sci.* **12** 3519–31
Serinaldi F, Bonaccorso B, Cancelliere A and Grimaldi S 2009 Probabilistic characterization of drought properties through copulas *Phys. Chem. Earth* A/B/C **34** 596–605
Serrano J and García R 2012 Assessment of drought risk perception in southeast Spain (Guadalentin river basin) (Spain: Department Of Geography, University Of Murcia)
Shaposhnikov D *et al* 2014 Mortality related to air pollution with the Moscow heat wave and wildfire of 2010 *Epidemiology* **25** 359
Sharma S and Mujumdar P 2017 Increasing frequency and spatial extent of concurrent meteorological droughts and heatwaves in India *Sci. Rep.* **7** 15582
Sheffield J and Wood E F 2012 *Drought: Past Problems and Future Scenarios* (London: Routledge)
Sheffield J *et al* 2014 A drought monitoring and forecasting system for Sub-Sahara African water resources and food security *Bull. Am. Meteorol. Soc.* **95** 861–82
Sheffield J, Wood E F and Roderick M L 2012 Little change in global drought over the past 60 years *Nature* **491** 435–8
Sillmann J, Kharin V, Zwiers F, Zhang X and Bronaugh D 2013 Climate extremes indices in the CMIP5 multimodel ensemble: II. future climate projections *J. Geophys. Res.: Atmos.* **118** 2473–93
Sklar M 1959 Fonctions de repartition an dimensions et leurs marges *Publ. Inst. Stat. Univ. Paris* **8** 229–31
Sousa P M, Trigo R M, Barriopedro D, Soares P M and Santos J A 2018 European temperature responses to blocking and ridge regional patterns *Clim. Dyn.* **50** 457–77
SPCCA 2016 Drought. Retrieved from (http://klimatanpassning.se/en/climate-change-in-sweden/temperature/drought-1.96659)
Stagge J H, Kingston D G, Tallaksen L M and Hannah D M 2017 Observed drought indices show increasing divergence across europe *Sci. Rep.* **7** 14045
Stagge J H, Tallaksen L M, Kohn I, Stahl K and Van Loon A F 2013 A European Drought Reference Database: Design and Online Implementation *Technical Report* no. 12 (Wageningen, the Netherlands: Drought R&SPI)

Teuling A J *et al* 2013 Evapotranspiration amplifies European summer drought *Geophys. Res. Lett.* **40** 2071–5
Tošić I and Unkašević M 2014 Analysis of wet and dry periods in Serbia *Int. J. Climatol.* **34** 1357–68
Trenberth K E, Dai A, Schrier G V D, Jones P D, Barichivich J, Briffa K R and Sheffield J 2014 Global warming and changes in drought *Nat. Clim. Change* **4** 17–22
Ulbrich U *et al* 2012 Climate of the Mediterranean: synoptic patterns, temperature, precipitation, winds, and their extremes *The Climate of the Mediterranean Region* (Amsterdam: Elsevier) pp 301–46
Veryard R 1956 Looking back on 1955 *Weather* **11** 83–8
von Buttlar J *et al* 2017 Impacts of droughts and extreme temperature events on gross primary production and ecosystem respiration: a systematic assessment across ecosystems and climate zones *Biogeosci. Discuss.* **15** 1293–318
Vázquez C, Zafra I and Olivares P 2016 Wild re on Spanish coast forces 1,000 people from their homes. Síguenos en Síguenos en Twitter Síguenos en Facebook Síguenos en Instagram (https://elpais.com/elpais/2016/09/05/inenglish/1473061956 870067.html)
Woollings T *et al* 2018 Blocking and its response to climate change *Curr. Clim. Change Rep.* **4** 287–300
Ye H 2018 Changes in duration of dry and wet spells associated with air temperatures in Russia *Environ. Res. Lett.* **13** 034036
Zhao T and Dai A 2015 The magnitude and causes of global drought changes in the twenty-first century under a low-moderate emissions scenario *J. Clim.* **28** 4490–512
Zolina O, Simmer C, Belyaev K, Gulev S K and Koltermann P 2013 Changes in the duration of european wet and dry spells during the last 60 years *J. Clim.* **26** 2022–47
Zscheischler J *et al* 2014 Impact of large-scale climate extremes on biospheric carbon fluxes: an intercomparison based on MsTMIP data *Glob. Biogeochem. Cycles* **28** 585–600
Zscheischler J, Orth R and Seneviratne S I 2017 Bivariate return periods of temperature and precipitation explain a large fraction of European crop yields *Biogeosci. Discuss.* **2017** 1–18
Zscheischler J and Seneviratne S I 2017 Dependence of drivers affects risks associated with compound events *Sci. Adv.* **3** e1700263
Zscheischler J *et al* 2018 Future climate risk from compound events *Nat. Clim. Change* **8** 469–77
Zurovec O, Vedeld P and Sitaula B 2015 Agricultural sector of Bosnia and Herzegovina and climate change-hallenges and opportunities *Agriculture* **5** 245–66